nature portfolio

https://doi.org/10.1038/s41586-021-03646-5

Supplementary information

Spectroscopic evidence for a gold-coloured metallic water solution

In the format provided by the authors and unedited

Supplementary Information:

Spectroscopic Evidence for a Gold-Coloured Metallic Water Solution

Philip E. Mason,[1†] H. Christian Schewe,[1,2†] Tillmann Buttersack,[1,2,3†] Vojtech Kostal,[1] Marco Vitek,[1] Ryan S. McMullen,[3] Hebatallah Ali,[2,4] Florian Trinter,[2,5,6] Chin Lee,[2,7,8] Daniel M. Neumark[7,8], Stephan Thürmer,[9] Robert Seidel,[10,11] Bernd Winter,[2] Stephen E. Bradforth,[3] and Pavel Jungwirth[1*]

[1]Institute of Organic Chemistry and Biochemistry, Czech Academy of Sciences, Flemingovo nam. 2, 16610 Prague 6, Czech Republic, [2]Molecular Physics, Fritz-Haber-Institut der Max-Planck-Gesellschaft, Faradayweg 4-6, D-14195 Berlin, Germany, [3]Department of Chemistry, University of Southern California, Los Angeles, CA 90089-0482, USA, [4]Department of Physics, Women Faculty for Art, Science and Education, Ain Shams University, Heliopolis, 11757, Cairo, Egypt, [5]Photon Science, Deutsches Elektronen-Synchrotron (DESY), Notkestr. 85, D-22607 Hamburg, Germany, [6]Institut für Kernphysik, Goethe-Universität Frankfurt, Max-von-Laue-Str. 1, D-60438 Frankfurt am Main, Germany, [7]Department of Chemistry, University of California, Berkeley, CA 94720, USA, [8]Chemical Sciences Division, Lawrence Berkeley National Laboratory, Berkeley, CA 94720, USA, [9]Department of Chemistry, Graduate School of Science, Kyoto University, Kitashirakawa-Oiwakecho, Sakyo-Ku, Kyoto 606-8502, Japan, [10]Helmholtz-Zentrum Berlin für Materialien und Energie, Albert-Einstein-Straße 15, D-12489 Berlin, Germany, [11]Humboldt-Universität zu Berlin, Department of Chemistry, Brook-Taylor-Str. 2, D-12489 Berlin, Germany

[*]Correspondence to: pavel.jungwirth@uochb.cas.cz

[†]All three authors contributed equally.

Table of contents:

1. Sample preparation and employment in the experimental setup

Rigorous safety measures are necessary at all times during handling, preparation, and disposal, as the sodium-potassium alloy (NaK) reacts violently with oxygen and/or water in the air. As a general safety standard, we clean any tubing or NaK containing vessel beforehand by evacuating or purging the containers and the tubing with rare gases or nitrogen to guarantee a water-free and oxygen-free environment.

Liquid NaK (1:1 atomic ratio at volumes up to 30 ml) was prepared in a flask filled with pentane by squeezing together pieces of solid sodium (Sigma Aldrich, 99.8 %) and solid potassium (Sigma Aldrich, 98 %) in a 1:1 molar proportion[1]. The formed liquid NaK was then safely handled using polypropylene syringes and hypodermic needles to transfer it into the reservoirs at the experimental setups. Any contact with halogen containing polymers (e.g., teflon) must be avoided, as these will spontaneously and violently react with NaK.

Recently, we built a liquid NaK microjet setup running in vacuum[2]. We achieved continuously running microjets by applying helium or argon on top of the NaK containing reservoir, which pushed the alloy through a polyethylene filter and a quartz nozzle

(diameter of ~80 µm) – the resulting microjets ran stably for tens of minutes until the NaK reservoir was empty. Here, in order to increase the interaction time with water vapour, we operated NaK jets at the lowest backing pressure possible. Within the present experiments, we found out that upon reducing the backing pressure to 0.1-1.0 bar relative to vacuum a stable train of NaK drops developed, which turned out to be particularly suitable for achieving a sufficiently long interaction with water vapour. Figure S1 depicts schematically the experimental setups that we manufactured to create continuously running drop trains of NaK for our optical and synchrotron x-ray photoelectron (PE) spectroscopy measurements.

NaK has a very low vapour pressure[3] – the partial pressures are $p_{Na} = 0.09 \cdot 10^{-6}$ mbar and $p_K = 0.91 \cdot 10^{-6}$ mbar at room temperature – which results in a total vapour pressure of $p_{NaK} = 1.00 \cdot 10^{-6}$ mbar. Therefore, practically no evaporative cooling happens which prevents the drop from freezing, unlike other (volatile) liquids like water or ethanol. Several major advantages can be exploited in this drop mode. First and foremost, compared to a jet the same

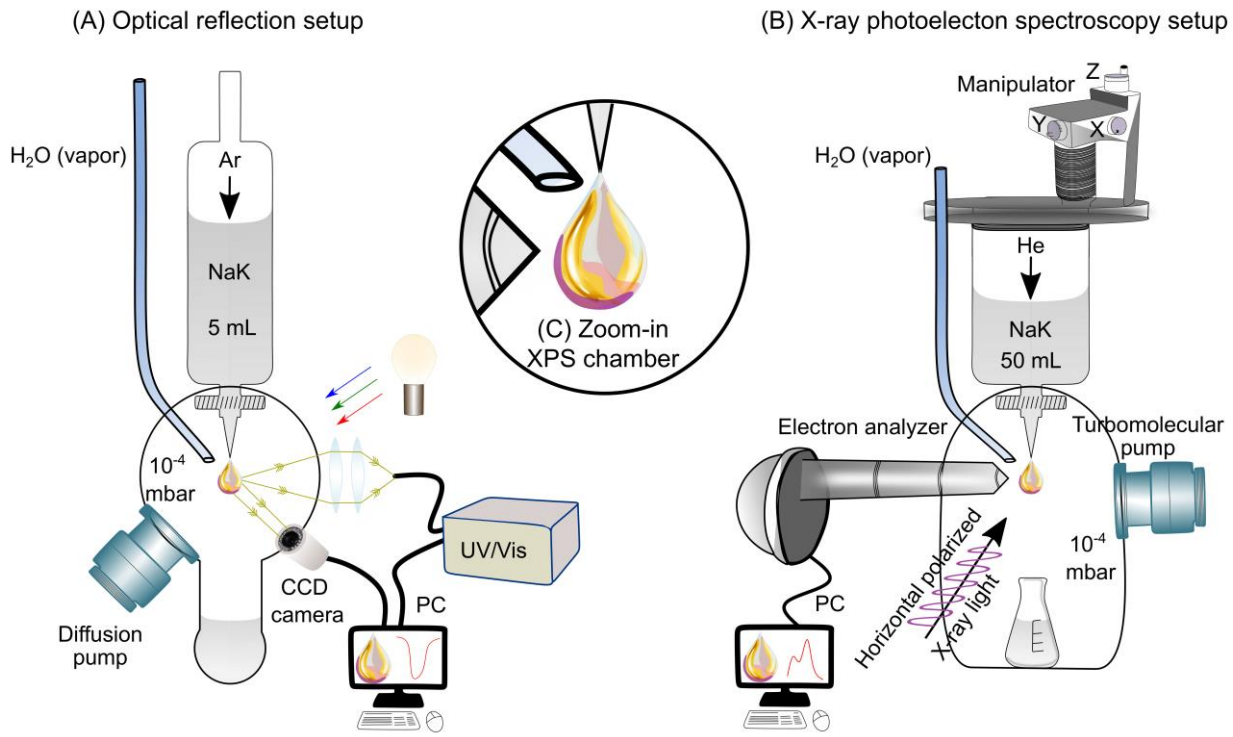

Figure S1: Sketch of the two different experimental setups used for the study of the metallic water solution. (A) Optical reflection setup. A train of NaK droplets was injected into a glass vacuum chamber under controlled humidity conditions. The reflection of white light was imaged into a UV/VIS-spectrometer while the state of the drop is recorded simultaneously with a CCD camera. (B) Scheme of the x-ray photoelectron spectroscopy vacuum chamber setup at the BESSY II synchrotron. The inset depicts a zoom-in of the NaK drop in the vacuum chamber.

surface spot interacts much longer with water vapour. Namely, assuming typical jet flow velocities of 50 - 100 m/s interaction times of only ~10 - 20 µs are realized if the probing spot is ~1 mm downstream of the capillary. In contrast, the lifetime of a drop can be set from several hundreds of milliseconds up to ~10 s, depending on the pressure applied on the top of the reservoir.

The probed NaK drops were collected in a glass beaker placed just below the reservoir (see Figure S1). As only the surface of the NaK drops had contact with water a large amount of the NaK alloy could be recycled and reused after each experimental run,

while the polyethylene filters, capillaries and syringes were disposed, after being cleaned with ethanol and quenched under safe conditions in water.

2. Photoelectron spectroscopy measurements

X-ray PE spectra were recorded at the U49-2_PGM-1 beamline[4] at the synchrotron radiation facility BESSY II, Berlin, Germany, using the SOL³PES experimental setup[5]. A polyethylene reservoir was mounted on a stainless-steel tube via a Luer-lock and was integrated into an *x*-*y*-*z*-manipulator (CF63, company VAb), see Figure S1 B). The NaK alloy was prepared as described in section 1 and filled into the polyethylene reservoir, which had been purged beforehand with helium to guarantee a water-free reservoir. Electrical grounding of the NaK sample was ensured by maintaining electrical contact between the grounded SOL³PES instrument and the liquid NaK sample, using a non-reactive platinum wire. At the Luer connection at the bottom of the reservoir, a poly-ethylene filter (pore-size of 0.45 µm) with a customized glass capillary was mounted[6]. NaK drops or jets were created by adjusting the helium backing pressure on the NaK reservoir as described in section 1.

Figure S1 shows schematically how NaK drops were irradiated on the upper part by horizontally polarized soft X-ray light and how the emitted photo-electrons were detected by a Scienta Omicron R4000 HiPP-2 hemispherical electron analyzer mounted in the plane of the polarization axis. There are three differential pumping sections, each consisting of a pinhole and two turbomolecular pumps, to separate the detector unit from the experimental chamber. A similar differential pumping scheme is used to generate the steep pressure difference between the experimental chamber and the ultra-high vacuum ($<10^{-9}$ mbar) inside the U49-2_PGM-1 beamline. PE measurements of pure NaK drops were performed at around 1.2×10^{-5} mbar.

PE spectra were recorded either using the sweep-mode or the fixed-mode acquisition setting of the Scienta Omicron hemispherical electron analyser. In the sweep-mode the spectrum is recorded by changing the voltages inside the electrostatic lenses in front of the hemisphere of the electron analyser in defined steps. Electrons having a kinetic energy that matches the predefined pass energy of the hemisphere are detected and a stepwise change of the lens retardation thus builds up the spectrum by sweeping a kinetic energy range of interest. In the fixed-mode all voltages are held fixed, allowing only for electrons around a single central energy to pass. The spectrum is thus measured by detecting the spread of kinetic energies around the central value at the 2D microchannel plate (MCP) detector of the electron analyser. The detectable spread depends on the size of the MCP and the selected pass energy of the hemisphere (+/- 4.5% of the electron analyser pass energy). This mode allows to measure all electrons within this pre-defined kinetic energy window at once without the need for sweeping voltages.

Spectra were recorded in the fixed mode at a repetition rate of ~0.6 Hz, i.e. one spectrum every 1.6 seconds – the actual recording of the electrons can be done as fast as ~20 *ms*, but a dead time for the read-out, pre-processing, and saving of the data limits the sampling rate. The recording of the same spectral interval by using the sweep-mode setting takes several tens of seconds with the obvious disadvantage that the whole spectral interval would not be recorded at once. Only the fixed-mode operation enables fast enough detection such that we trace the changes in the electronic structure once the water vapour starts reacting with pure NaK to form alkali hydroxide, which happens within the first 2 - 5 seconds of the drop's lifetime. Therefore, unless stated otherwise, measurements were performed in the fixed mode.

The PE energy resolution is determined by the U49-2_PGM-1 beamline settings, which was better than 120 meV for our measurements at 310, 320, and 330 eV photon

energies, and by the energy resolution of the electron analyzer, which was ~125 meV for the measurements at a pass energy of 100 eV.

3. Photoelectron spectra of pure NaK jets versus drops

Figure S2 depicts valence band PE spectra from a pure continuously flowing NaK jet (blue solid line) and from a train of drops (red solid line) measured in sweep mode at a photon energy of 310 eV. There is a non-zero intensity present at negative binding energies, which we attribute to an inelastic electron background tail resulting from potassium $2p_{1/2,3/2}$

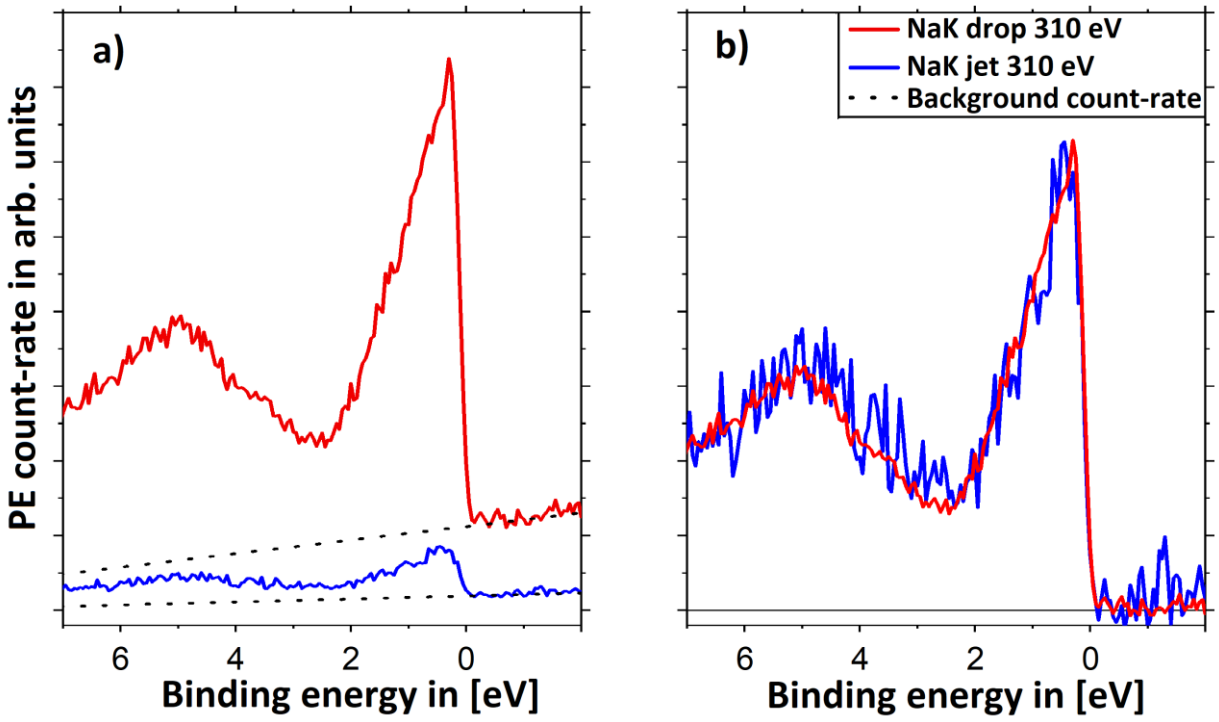

Figure S2: PE spectra of a NaK jet (blue) and of a drop (red) measured at a photon energy of 310 eV: a) Raw spectra, b) after subtraction of a linear background (see also Figure S3) and normalization the spectra are identical with the drop spectrum having a much better S/N ratio. Binding energies are referenced to the Fermi edge.

at 297 and 294 eV binding energy, respectively, irradiated with (unavoidable at the beamline used) 2nd harmonic light of 620 eV from the undulator. To further elucidate the background, we measured a valence band spectrum of a pure NaK jet in the sweep

mode at a photon energy of 320 eV. Here, we extended the observed binding energy window to -30 eV (see Figure S3). The photoelectrons resulting from ionization by the 2nd harmonic radiation possess a kinetic energy of ~323 eV ($2p_{1/2}$) and ~326 eV ($2p_{3/2}$), which corresponds to a binding energy of -23 eV and -26 eV, respectively. This assignment was further strengthened by overlaying the extended valence band spectrum with a shifted potassium 2p spectrum measured at a photon energy of 700 eV from a NaK jet. Notably, the long tail upon ionizing with the 2nd harmonic light shows oscillating behavior, which is due to the related plasmon peaks. By comparing our spectra with data from Bonzel et al.[7] from adsorbed potassium on a Pt(111) single crystal in contact with or without water we could identify small contributions of potassium hydroxide 2p peaks, which are blue-shifted by ~1.5 eV from their pure potassium metal counterparts.

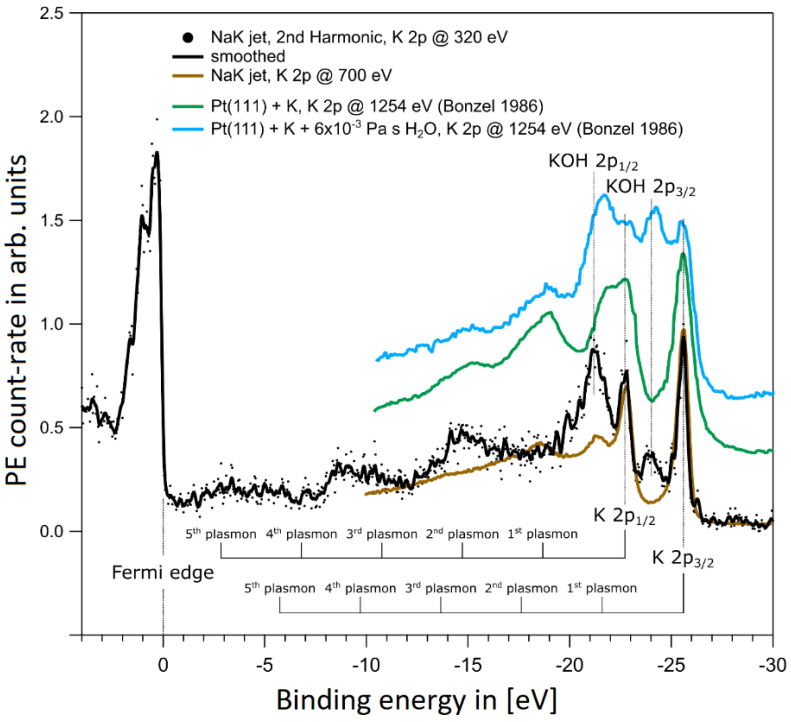

Figure S3: Extended valence band spectrum of a pure NaK jet measured in sweep mode (black dots, smoothed – black line) exhibits the 2nd harmonic features the potassium 2p peaks. The oscillating tail towards lower negative binding energy (lower kinetic energy) is due to plasmonic peaks related to the K $2p_{1/2;3/2}$ peaks. PE contributions from KOH $2p_{1/2;3/2}$ are indicated and identified by measurements from Bonzel et al.[7] (blue curve).

To reduce the count-rate of this (unwanted) background from the potassium 2p 2nd harmonic peaks and the respective plasmon peaks we performed all the NaK+H_2O measurements reported here at a photon energy of 330 eV. After subtraction of a linear background the PE spectra of NaK drops and of a NaK microjet perfectly overlap when applying a single scaling factor (see Figure S2B).

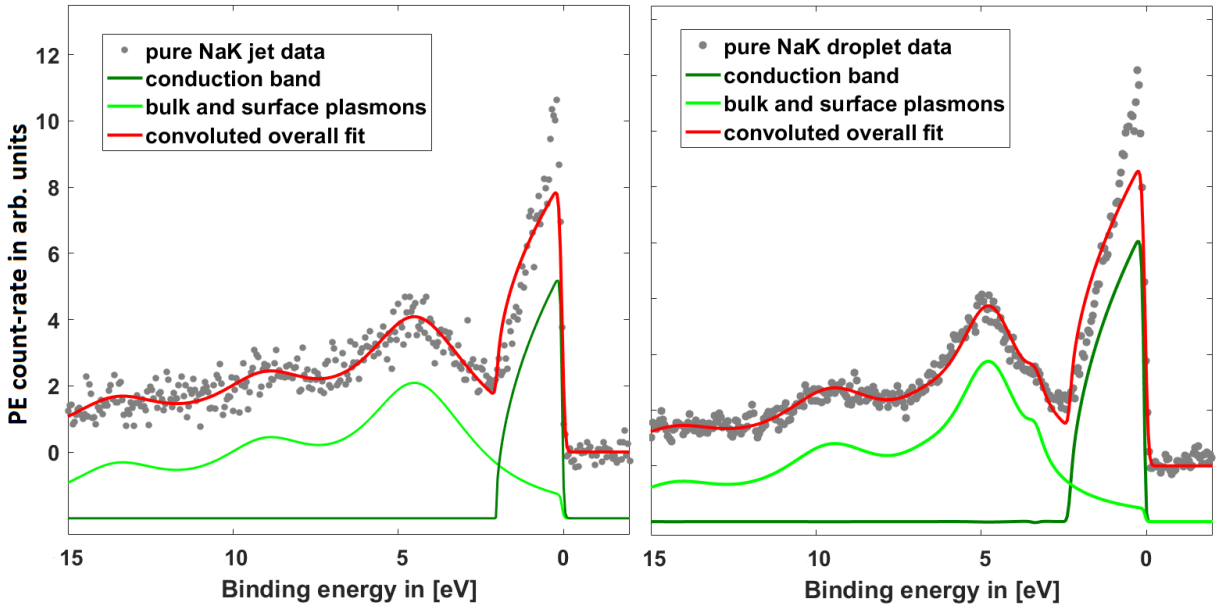

Figure S4: Valence band PE spectra of a continuously running NaK microjet (left) and of NaK drops (right) with the fitted results from the free electron gas model included as solid lines: the red solid line is the overall fit, resulting from the substructures of the conduction band between 0 and 2 eV (dark green solid line) as well as the first, second and third bulk plasmon peaks (light green solid line), respectively. In the spectrum of NaK drops even the first surface plasmon (at ~3.4 eV) can be identified and fitted due to the better signal-to-noise ratio relative to the jet spectrum.

The NaK drop spectrum has a much better signal to noise ratio than the NaK microjet spectrum, which is primarily due to longer integration times. The NaK valence PE spectrum can be fitted using the free electron gas (FEG) model. The width of the

conduction band as well as the position of the plasmon peak can be predicted based on the electron density (n = 1.79×10^{22} cm^{-3} for an atomic ratio of Na:K = 1:1) - for further details see section 7 of this SI and references therein. Figure S4 depicts fits of the conduction band, as well as the plasmon peaks for the NaK drop and jet spectra. For both the conduction band (dark green fit) is found to be approximately 2 eV wide, while the first, second, and third bulk plasmon peaks are identified at around 4.8, 9.6, and 14.4 eV, respectively.

4. Photoelectron spectra of water vapour adsorbing on the NaK drop surface

To measure PE spectra of the metallic water solution, we used the experimental setup depicted in Figure S1B. The water vapour capillary was mounted onto the same *x*-*y*-*z*-manipulator as the NaK reservoir – which allowed a simultaneous adjustment of the NaK drop position and the water vapour capillary. A needle valve was used to adjust the required H_2O gas flow. The reservoir of the degassed milli-Q water could be heated to increase the water vapour pressure. Upon opening the water vapour reservoir, the pressure in the experimental chamber increased from 10^{-5} mbar to ~10^{-4} mbar, although locally the partial H_2O pressure at the NaK surface was likely somewhat higher, because the effusive beam of water vapour from the capillary was directed onto the upper part of the forming NaK drops.

The distance between the electron analyzer entrance (500 µm diameter orifice) and the irradiated surface spot (~80 x 115 µm in diameter) was approximately 500 µm. This short distance ensures that any electron signal is hardly reduced by inelastic electron scattering due to the locally elevated water vapour pressure. The rather high photon energy of 330 eV was necessary to create valence (or conduction band) photoelectrons with kinetic energies above 300 eV, which allowed us to use a pass energy of 100 eV. This large pass energy was essential to collect a 9-eV wide spectral interval (i.e., +/-

4.5 % of the pass energy) in a single shot using the fixed-mode setting in our electron analyzer/2D-MCP-CCD detector unit. By design, the measured kinetic energy of the electrons (adjustable by the photon energy) must be at least three times larger than the pass energy used in our R4000 HiPP-2 electron analyzer. Although this is a rather unconventional mode of measuring PE spectra, it is the only viable option to trace the spectral changes due to the drop dynamics, including changes in size, happening on a timescale of a few seconds. In fixed-mode operation, we chose to integrate for ~0.4 seconds, with a snapshot of the 9 eV wide spectral interval being recorded simultaneously. Including the dead time of 1.2 *s* for read-out, pre-processing, and saving of the data we acquired a spectral snapshot every 1.6 s, which corresponds to a sampling rate of ~0.6 Hz. It allowed us to reach
an acceptable signal-to-noise ratio for one spectral snapshot, but it is also short enough to resolve in full detail individual steps of the process (as we did within the optical measurement). Within a typical drop lifetime of ~10 seconds we generate 6-7 spectral snapshots and in a whole experimental run a train of drops was measured over a time of ~20 minutes (corresponding to ~100 drops).

5. Data-analysis of photoelectron spectra acquired in fixed-mode operation

5.1 Evaluation of time-resolved data sets acquired in fixed-mode operation

Figure S5 shows the raw data of a series of valence PE spectral snapshots from a NaK drop train exposed to water vapour that was recorded in fixed-mode operation – consecutive spectral snapshots are depicted ‘as measured‘, with the PE count rate plotted against the binding energy for each spectral snapshot. Note that the binding energy axis has not been calibrated at this stage. This plot illustrates the periodic pattern of the drop evolution from the built-up until the fall-off from the nozzle, which is best seen by the

intensity variation of the hydroxide peak at high binding energies. The drop repetition rate in this measurement is roughly one drop every 10 seconds. Ideally, the drop rate is constant during the measurement. However, the lifetime of the drops may slightly vary over time because the polyethylene filter and the self-made quartz capillary mounted at the end of the NaK reservoir partially clog throughout each experimental run. Also, varying drop lifetimes in different experimental runs are primarily due to slightly different diameters of our self-made capillaries.

We implemented protocols and scripts in MATLAB and Python (version 3.7.6) that check for spectral snapshots at which new NaK drops start emerging. Figure S6 depicts the integrated PE count rate plotted as a function of the number of consecutively recorded spectral

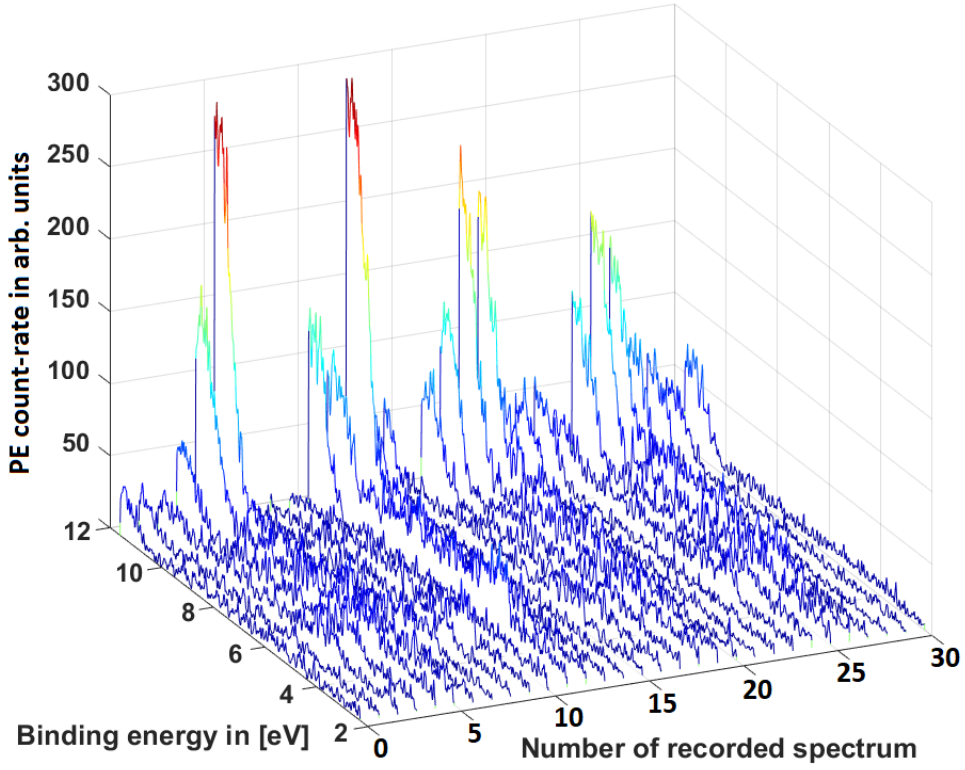

Figure S5: 30 spectral snapshots of valence PE spectra from a NaK drop train illustrating the data-acquisition in fixed-mode operation. This series of snapshots cover roughly 40 seconds of measurement time, equivalent to the lifetime of four drops. Note: the binding energy axis is not calibrated.

snapshots. We used the fact that the PE count rate integrated over the whole fixed-mode binding energy interval decreases practically to zero once a drop has fallen off, since there is no target for the x-ray beam to create photoelectrons. We define the starting point of a new NaK drop between the two consecutively acquired spectral snapshots where the integrated PE count rate starts to increase again. The red crosses represent the spectral snapshots that have been taken just before the integrated PE count rate starts to increase, i.e., when a new drop emerges, marking t = 0.0 s. The remaining labels mark consecutive snapshots sampled at 1.6, 3.2, 4.8 *s*, etc. – the same colour marker indicates a similar stage of the drop lifetime.

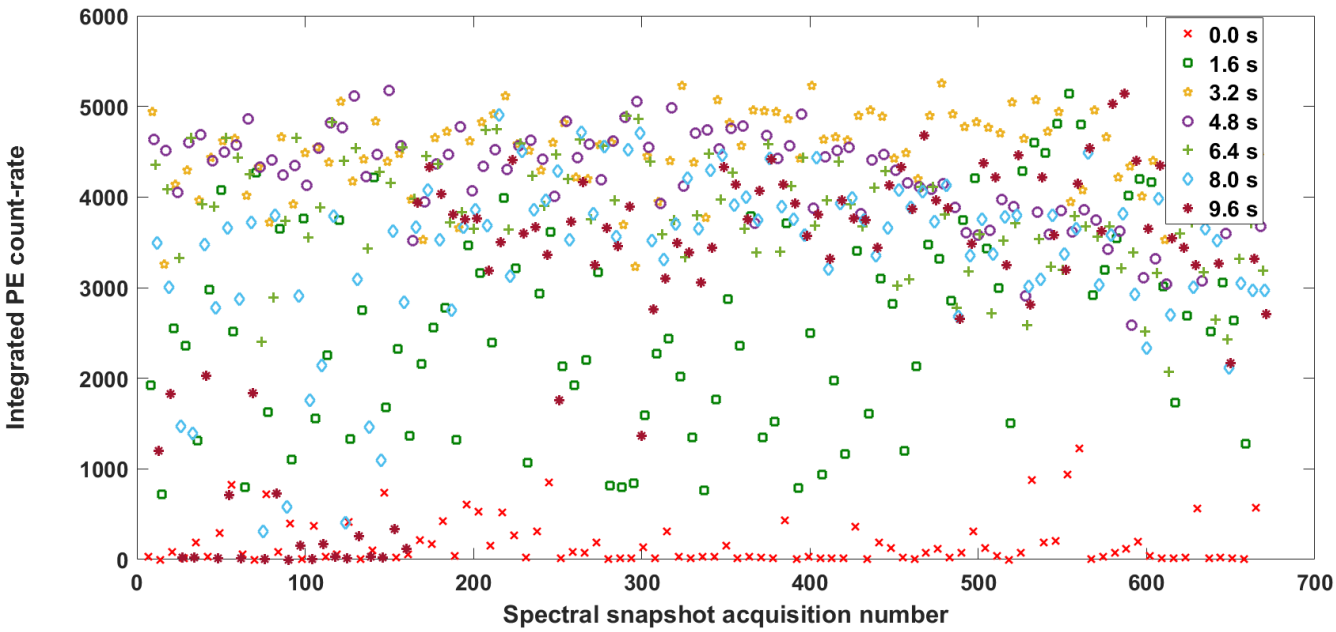

Figure S6: integrated PE count rate of each individual spectral snapshot is plotted against its spectral snapshot acquisition number. The red crosses mark each spectral snapshot taken just before the formation of a new drop. The coloured markers symbolize spectral snapshot corresponding to the same temporal delay relative to the beginning of the drop formation.

The left part of Figure S7 depicts all spectral snapshots of a typical experimental run after grouping them corresponding to the time interval in which they have been

acquired relative to the formation of a new drop. In this way, we achieve a temporal resolution defined by the sampling rate of the acquisition of the spectral snapshots in the fixed-mode. The change of the valence band spectra directly reflects the evolution of the NaK drop surface under the influence of the adsorbed water vapour. As shown in Figure 1 of the main manuscript, the overall development in the drop's 'life' is about the shiny metallic NaK surface turning gold and eventually into white crusty insulating hydroxide. This can also be observed in the valence PE spectra where in the beginning the metallic features which are most prominently represented by the conduction band between 0 eV and 2 eV binding energy decrease within the first 5 seconds until they finally disappear after ~8 s. The presence of plasmonic features is indicated by the shallow peaking of the PE count-rate at around 4.5 eV, which we assign to the first bulk plasmon of NaK. A second plasmonic peak around 2.7 eV is only present in the spectra corresponding to 1.6, 3.2, and 4.8 *s*. We assign this feature to the bulk plasmon of

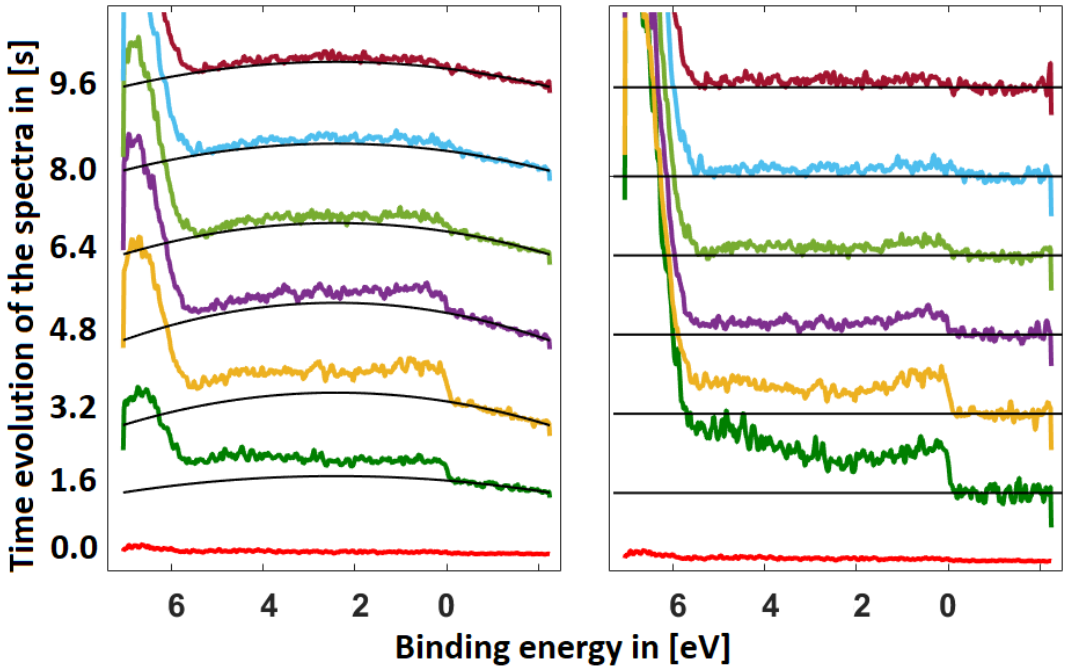

Figure S7: left and right part show valence PE spectra plotted against the binding energy with respect to the Fermi edge. The spectra show an average after grouping spectral snapshots which have been recorded within the same temporal interval relative to the NaK drop's beginning at 0.0 s. Looking at the spectra upwards along the vertical axis reflects the evolution of an average NaK drop as a function of time. The black lines in the left part represent an inverse parabola fit to each spectrum indicating a differently distributed underlying count rate which quantitatively changes as time progresses but qualitatively remains the same. The right part shows the same spectra after the correction procedure for the parabolic background has been applied that is described in subsection 5.2 in detail.

the metallic water solution, since it is only present during the times when the drop is predominantly golden.

In contrast to the metallic spectral features that diminish in time, a peak emerges around ~7 eV binding energy and becomes the only feature remaining in the spectrum at later times. We assign this peak to hydroxide as a product of the chemistry. Note that

corresponding literature values for alkali hydroxides formed on alkali metals vary between 6 to 7 eV binding energy with respect to the Fermi edge[7-9], while the corresponding value for aqueous hydroxide was reported with respect to the vacuum level only[10].

5.2 Characterization of the count rate in fixed-mode operation

When looking at the time-resolved spectra in Figure S7 we see that there is a 'pedestal-like' count rate underlying in each spectrum. Additionally, the count rate of the spectral intensities in the centre of the interval seem to be exaggerated while that towards the borders is undervalued. Both tendencies are indicated by an underlying inverse parabola in Figure S7. This behaviour can be observed particularly well in to the right from the Fermi edge, where there is little signal. The non-zero count rate for binding energies below the Fermi edge has already been assigned to the inelastic electron background tail resulting from potassium 2p1/2,3/2 PE peaks and corresponding plasmons when irradiated with a 2nd harmonic x-ray light (compare with Figure S3). Note that in the sweep-mode spectra shown in Figure S2, the count rate of this background decreases with increasing binding energy, while in the fixed-mode spectra it shows the opposite behaviour, i.e., the background count rate increases with increasing binding energy. Moreover, we observe the count rate to vary in intensity and the underlying parabola-like pedestals to show a varying curvature depending on the stage in the lifetime of the drop. In order to characterize this behaviour in more detail we used a series of fixed-mode spectra recorded at the end of a scan.

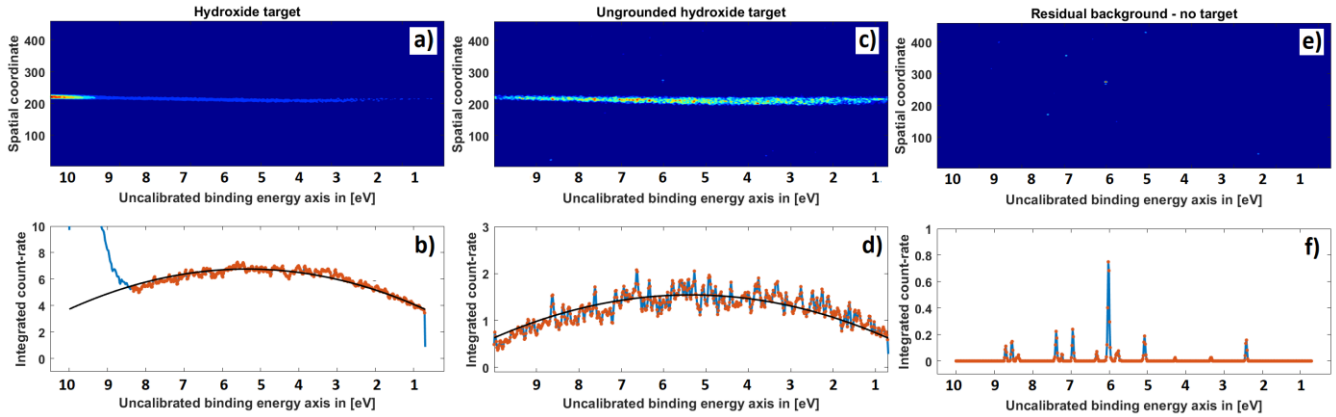

Figure S8: Upper row shows actual images taken by the CCD camera, while the bottom row shows the count rates integrated along the (vertical) spatial axis as a function of the binding energy.

If photoelectrons propagated ideally through the electrostatic lens arrangement and then the hemispherical analyzer, they are imaged onto a straight line on the MCP in the position-resolved mode. The actual count rate recorded with the CCD camera corresponds to an image where the horizontal dimension corresponds to the kinetic energy coordinate, while the second (vertical) dimension corresponds to a spatial coordinate as is shown in the top row of Figure S8. The line on the MCP represents the image of the small skimmer orifice in spatial direction; a larger orifice or larger magnification settings would give a broader line. The typical spectra, where the count rate is plotted as a function of the binding energy is derived by integrating the count rate along the spatial dimension, as depicted at the bottom row of Figure S8.

Figure S8a shows a valence PE spectrum of the hydroxide-covered drop, where the only spectral feature is the hydroxide peak at high binding energy. There is however additional count rate toward lower binding energies lower. This additional count rate exists due to the higher-harmonic ionization of the potassium $2p_{1/2,3/2}$ as described in section 4. As time progresses also the hydroxide peak disappears from the spectrum, see Figure S8cd. Since the hydroxide layer does not physically disappear, the vanishing signal must be attributed to this thick layer being poorly electrically conducting, which

leads to charging of the surface upon x-ray irradiation and hence smearing out of the sharp PE peaks.

In both graphs, it is also clearly visible that the count rate in the centre of the spectral interval (i.e., in the centre of the MCP) is emphasized. The manufacturer of the electron detection system has indicated that this is due to the fact that the lens that images phosphorescence onto the CCD can produce blurring away from the image center. Additionally, we identified a number of instrument-inherent properties that enhance this effect. When analyzing the raw detector data, we observed that the count rate is not imaged perfectly along a straight horizontal line as can be observed qualitatively in Figure S8ab. This deviation is most likely caused by the imperfectly compensated magnetic field using Helmholtz coils[5], which result in imaging errors of the PE trajectories onto the entrance slit of the hemispherical electron analyzer. These circumstances would quantitatively result in a lower (or higher) probability for PE to be transmitted through the electro-static lens and the hemispherical analyzer if they are imaged towards the outskirts (or centre) of the MCP. In order to quantify this behaviour, an inverse parabola has been fit to the data. As a crosscheck that this parabolic count rate is not resulting from some dark count rate present in any experiment due to cosmic rays or natural radioactive decay, the target has been moved out the x-ray beam. The residual dark count rate is depicted in Figure S8ef.

In summary, we can practically account for this intensity scaling of signal across the MCP/CCD as follows:

1. We first average the spectral scans at the same drop lifetime.
2. We fit an inverse parabola to the data set. For many datasets, the fitting can only be performed in the interval from the Fermi-edge toward lower binding energies, where the PE signal should be zero.

3. We divide the count rate as a function of the binding energy by the fitted parabola to correct for the intensity scaling. Afterwards, we account for the background count rate resulting from the potassium 2P $_{½,3/2}$ as described in section 4.

Figure S9 shows two examples how this protocol transforms the count rate intensities of fixed-mode spectra into spectra that would be acquired (if possible) using sweep-mode. The left graph shows the correction procedure for the hydroxide data that are also shown in Figure S8a. The right part shows the fixed-mode correction protocol applied to a dataset where the valence band of pure NaK has been measured. Figure S9b illustrates the fixed-mode spectrum and the parabolic fitting to it. Figure S9c shows the corrected spectrum in red, which can be compared to a similar spectrum in sweep-mode plotted in blue.

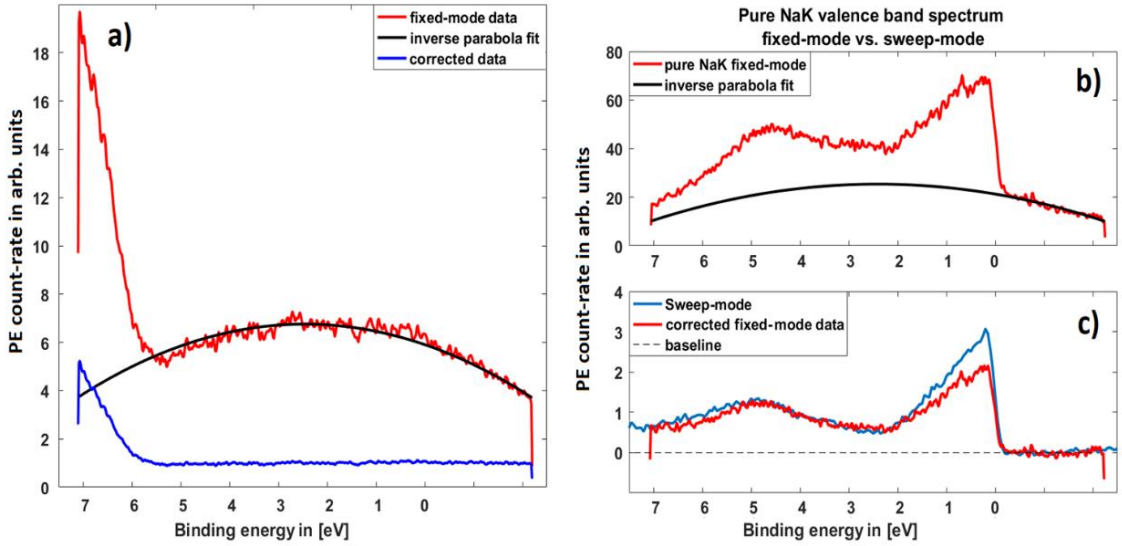

Figure S9: The left part shows the correction procedure for the hydroxide data (that are also shown in Figure S8). The right part shows the fixed-mode correction protocol applied to a data set where the valence band of pure NaK has been measured. The top part illustrates the fixed-mode spectrum and the parabolic fitting to it. The lower part shows the corrected spectrum in red, which can be compared to a similar spectrum in sweep-mode.

5.3 Evaluation of spectra in fixed mode operation

In order to increase the signal to noise ratio, we have been averaging the spectral snapshots acquired in fixed-mode after the temporal grouping as described in subsection 5.1. After application of the correction procedure described in subsection 5.2 we can add up the corrected spectral intervals regardless if they have been taken within the same experimental run (with several hundreds of drop formation events) or those recorded in different experimental runs. Figure S10 depicts as an example the averaged time-resolved spectra of a typical single experimental run. The final spectrum collected by summing up individual spectra corresponding to early times (roughly first two seconds) of the drops' developments from multiple experimental runs is then presented as black dots in Figure S12 (and Figure 4b of the main manuscript).

One can see already from the single experimental run the two key features characteristic for a metallic water solution – a plasmon peak at around 2.7 eV and a narrow (~1.1 eV) conduction band on top of the roughly twice as wide conduction band of NaK (both ending with a sharp Fermi edge at 0 eV) – appear in the spectra at an early stage of the drop development when its surface is gold-coloured (blue and red lines in Figure S10, right). In addition, one can clearly see a slight shift in time of the onset of the hydroxide peak at high binding energies (Figure S10, left) indicating increasing concentrations of aqueous hydroxide[10] as chemistry proceeds during the maturation of the drop.

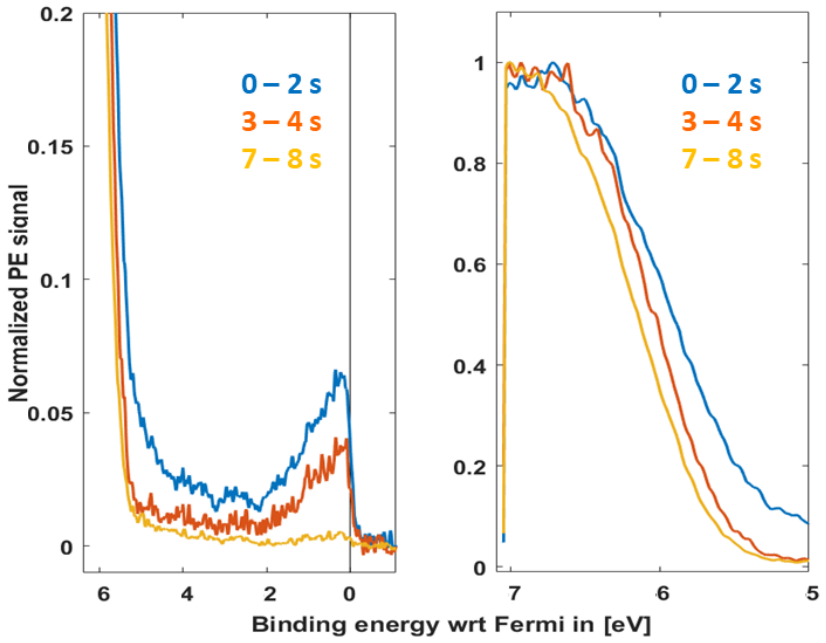

Figure S10: Spectra collected from a single experimental run recorded in the fixed mode at early (blue), intermediate (red), and late (yellow) stages of the development of the drop. Left: full time-resolved fixed mode spectra. Right: zoomed in onset of the hydroxide peak at high binding energies.

5.4 Spectral signatures of liquid water in sweep-mode spectra

Figure 11a depicts valence band spectra recorded in the sweep-mode. The red and black curves depict the spectral intensity distribution of averaged sweeps of NaK drops in the presence of water vapour pressures of 10^{-4} and 10^{-5} mbar, respectively. The average measurement time of one sweep corresponds to an integration over ~20 drop lifetimes. The binding energy axes of the red and black spectra are referenced to the Fermi level E_F = 0 eV, while their spectral intensities have been scaled. The golden doted curve represents the residuals of the red and the black curves. In Figure 11b the PE spectral interval (0 - 7 eV) covered during the fixed-mode data-acquisition is plotted as green curve, showing a reasonable agreement within the noisier residuals of the red and the black curves which are plotted again as golden dots. In order to achieve a better

comparison with the sweep-mode spectral intensity distribution the fixed-mode data sets over the whole lifetime of the drop are plotted. A second comparison is made using the known spectral intensity distribution of pure liquid water[11] which is depicted as blue curve. The agreement between the golden and the blue curves is quantitative, which clearly suggests that liquid water is present on the surface of the NaK drop. We have manually shifted the x-axis of the blue spectrum since we cannot reference its binding energy axis relative to the Fermi-level. However, the fact that the binding energy position of the liquid $1b_1$ peak is located at slightly higher binding energies relative to the hydroxide peak is a strong indication that its spectral position is correct.

It is important to stress that we acquired this spectrum in sweep-mode which does not allow any temporal resolution of when the liquid water is present during the lifetime of the drop. But the fact that there are spectral signatures of liquid water proves that it must be there at least for some time during the lifetime of the drop.

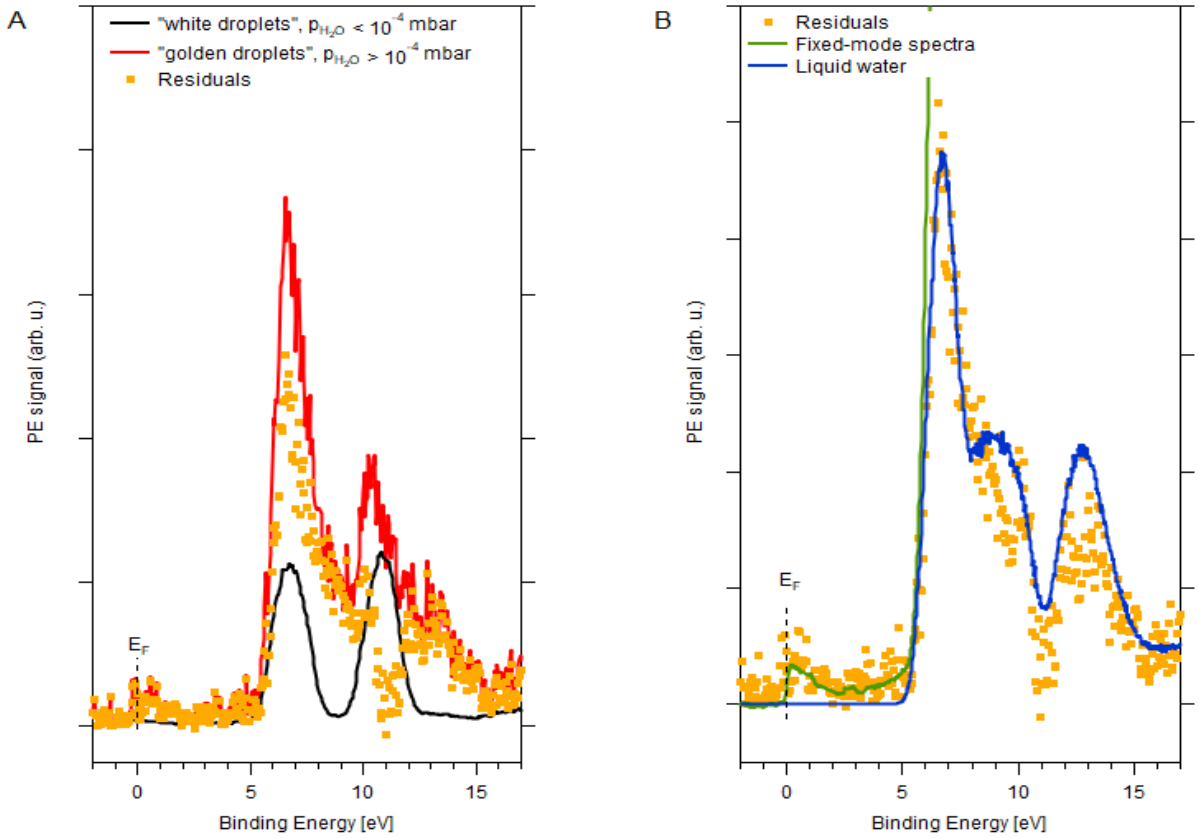

Figure S11: a) the red and black curves depict valence band spectra which have been recorded in the sweep-mode. The spectral intensity distribution of averaged sweeps of NaK drops in the presence of water vapour with pressures greater and smaller ~10^{-4} mbar, respectively. The average measurement time of one sweep corresponds to an integration over ~20 drop lifetimes. The binding energy axis of the red and black spectra are referenced to the Fermi level E_F = 0 eV. The golden doted curve respresents the residuals of the red and black curves. b) Comparison of the residuals to fixed-mode spectra (green) and to the pure liquid water spectrum[11].

6. Data-fitting of photoelectron spectra

In the following, a fitting procedure is described which is an adaption of procedures and routines that have been specified, for instance, in the SI of Ref. 2 and references therein. A designed fit-function is used as an input for a non-linear, least-square optimization routine, where an initial set of parameters is adjusted in a non-linear

regression until a parameter set has been determined that fits the measured data set optimally.

As we know from the CCD camera pictures and the optical spectra, when the NaK drop is exposed to water vapour, we observe the surface not to be entirely golden (which we identified as the metallic water solution in the optical spectra), but there can also be parts of pure NaK or hydroxide on the surface of the drop. Consequently, the fitting function consists of three components. Namely, we address the hydroxide peak using a Gaussian function while we account for the spectral features of the metallic water solution in an analogous way as we did when fitting pure NaK spectra (see Figure S4), where we used FEG[12]. Therein, the conduction band is represented by the function of the density of states (DoS) that has a square-root dependence as a function of the binding energy E_{bind}:

$$\mathrm{DoS}(E_{\mathrm{bind}}) = \frac{A_{\mathrm{DoS}}}{2\pi^2}\left(\frac{2\mathrm{fm}_e}{\hbar^2}\right)^{3/2}\sqrt{E_{\mathrm{bind}} - E_F(f)}.$$

where m_e is the electron mass and $\hbar$ *is* Planck's constant. A_{DoS} and f are parameters in the fit

accounting for the intensity and the effective electron mass. $E_F(f)$ is the Fermi-energy, which denotes the energy spacing between the bottom of the conduction band up to the Fermi

edge and is given by:

$$E_F = \frac{\hbar^2}{2\mathrm{fm}_e} \cdot (3\pi^2 n_i)^{2/3},$$

where n_i (i = *MW* or *NaK*) stands for the free electron density of the metallic water solution or NaK. In the case of NaK, n_{NaK} can be derived from the mass density and the chemical composition of the

individual liquids[13].

A second feature in metallic spectra are plasmon peaks, which are typically observed at higher binding energies relative to any occupied state in metals resulting from

inelastic scattering of outgoing photoelectrons with the free electron plasma in the conduction band. We model the plasmon peaks using a Lorentzian function[14]:

$$\mathrm{Pl}_{\beta}(E_{\mathrm{bind}})=\mathrm{A}_{P}\left(\frac{\gamma}{(E_{\mathrm{bind}}-E_{P})^{2}+\gamma^{2}}\right),$$

where A_p and γ are fit parameters accounting for the intensity and the width of the distribution.

The energy E_p of the plasmons is given by multiples of β = 1,2,3,… while the bulk plasmon

energy is given by $E_p^b=\beta\hbar\omega_p$ and of the surface plasmon energy by $E_p^s=\beta\hbar\omega_p/\sqrt{2}$.

The plasmon frequency is given by:

$$\omega_p=\sqrt{\frac{n_{\mathrm{MW/NaK}}e^2}{\mathrm{fm}_e\varepsilon_0}},$$

where ε_0 is the dielectric vacuum permittivity. Thus, we are using the following fit-function:

$$\mathrm{MFF}(E_{\mathrm{bind}})=\left[\mathrm{DoS}(E_{\mathrm{bind}})+\mathrm{Pl}_{\beta=1}^{(b)}(E_{\mathrm{bind}})\right]\cdot\mathrm{FD}(E_{\mathrm{bind}}).$$

for the metallic spectral features, where $FD(E_{bind})$ is the Fermi-Dirac probability distribution.

It resembles the sharp population cut-off at low binding energies, given by:

$$\mathrm{FD}(E_{\mathrm{bind}})=\left(1+\exp\left[\frac{E_{\mathrm{bind}}-E_{\mathrm{FE}}}{\mathrm{kT}}\right]\right)^{-1}.$$

Throughout the fitting we set the temperature to $T = 293\ K$, which correspond to the temperatures during the measurements and the position of the Fermi edge at $E_{FE} = 0$. The hydroxide features in the PE spectra are modeled using a single Gaussian function

$$\mathrm{Hyd}(E_{\mathrm{bind}})=\mathrm{A}_{\mathrm{Hyd}}\exp\left[\frac{E_{\mathrm{bind}}-E_{\mathrm{Hyd}}}{2B_{\mathrm{Hyd}}}\right]^{2},$$

where A_{Hyd}, E_{Hyd} and B_{Hyd} are fit parameters for the intensity, the center and the width of the Gaussian function.

We assume in the fitting model that the PE intensity of the spectral features of

both liquid metals - pure NaK and metallic water solution - are additive because the count rates as functions of the binding energy sum up. Since the two metals have physical contact they are both grounded with the PE-analyzer, hence their Fermi edges align at the same binding energy. Additionally, in the optical spectra we have observed the plasmon peak of the metallic water solution at ~2.7 eV, compared to a value of ~4.5 eV for pure NaK. This indicates that the two liquid metals have different electron densities leading not only to different binding energies of the plasmon peaks but also to different widths of the conduction bands. Thus, we use in the general fit-function *GFF(E_{bind})* two separate metallic

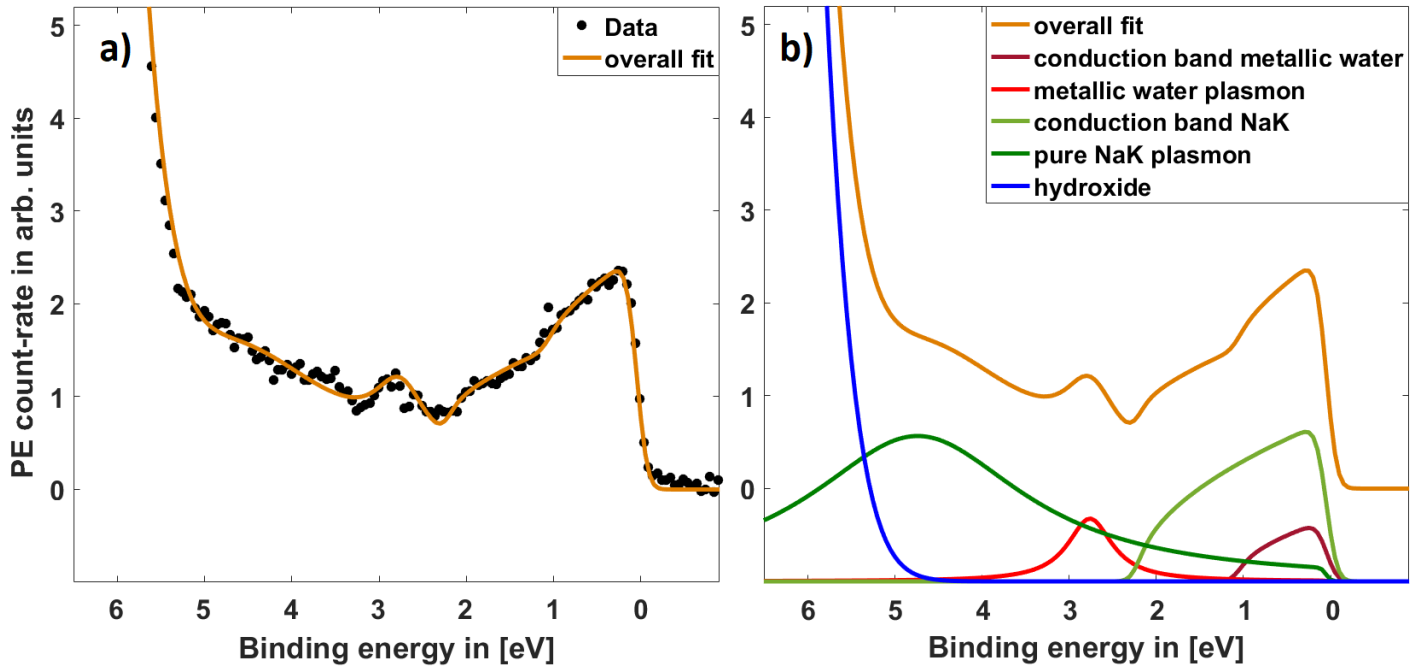

Figure S12: a) The collected experimental data are fitted using the free-electron model for both metallic species, i.e., metallic water solution and NaK. b) The fits to the spectral features of both metals are additive. Both align energetically at the Fermi edge, the different electron densities lead, however, to different widths of conduction bands and positions of the first bulk plasmon peaks. The conduction bands and the plasmon peaks of the metallic water solution are fitted using the FEG model assuming a Lorentzian function for the plasmons.

fitting functions to account for two conduction bands and two plasmons:

$$\mathrm{GFF}(E_{\mathrm{bind}}) = [\mathrm{DoS}_{\mathrm{MW}}(E_{\mathrm{bind}})+\mathrm{DoS}_{\mathrm{NaK}}(E_{\mathrm{bind}})+\mathrm{Pl}_{\mathrm{MW}}(E_{\mathrm{bind}})+\mathrm{Pl}_{\mathrm{NaK}}(E_{\mathrm{bind}})+\mathrm{Hyd}(E_{\mathrm{bind}})]\cdot\mathrm{FD}(E_{\mathrm{bind}}),$$

where we account for the hydroxide intensity as well. The overall fit-function *OFF(E_{bind})* that is used as input in the fitting routine is thus

$$\mathrm{OFF}(E_{\mathrm{bind}}) = [\mathrm{GFF}(E_{\mathrm{bind}})\otimes \mathrm{G}_{\mathrm{res}}(E_{\mathrm{bind}})],$$

where *GFF(E_{bind})* is convoluted with the instrumental resolution function *G_{res}(E_{bind})*.

Figure S12 shows the data set derived in the evaluation process (black dots), described in section 5, together with the fit-result of the overall fitting function *OFF(E_{bind})* as solid light brown line, while the separate fits of the individual spectral features are plotted at the bottom of the graph. Table S1 presents the results of the fitting procedure after the routine has optimized the parameters in *OFF(E_{bind}).*

Table S1: Fitted values of the plasmon peak position E_p and width (FWHM), width of the conduction band E_F, and free electron density n_e. Second row: fitting results using the FEG model after fitting OFF(E_{bind}) to the data-set illustrated in Figure S12. Third row: fit of a Lorentzian function to the absorption band in the optical reflection spectrum (Figure S14c).

	E_P [eV]	FWHM plasmon [eV]	E_F [eV]	n_e [cm^{-3}]
PE spectroscopy	2.76	0.62	1.14	5.52×10^{21}
Optical spectroscopy	2.74	0.59		5.44×10^{21}

7. Optical reflection spectroscopy

Exposing NaK drops to water vapour induces a colour change (from silver to yellow with a golden metallic sheen) that we probe using optical spectroscopy. The colour of metals interacting with electromagnetic (EM) radiation is determined[15] by their plasmon

resonance frequency (ω_P), as smooth metal surfaces will reflect EM radiation with frequencies (ω) up to the plasmon resonance frequency ($\omega \leq \omega_P$) and become transparent beyond this (i.e., $\omega > \omega_P$; see scheme in Figure S13a). Pure NaK, consisting of two simple metals, has no optical inter-band transitions and thus no visible light absorption[12].

Upon exposure to water, a layer of a metallic solution forms on the NaK drop and grows in thickness at a rate of ~24 nm/s (see main text). Within the first ~5 seconds during which the drop is gold-coloured, the metallic solution thus reaches a thickness of ~120 nm that is below the 200-800 nm wavelength range used in our optical investigations. The free electron densities determined by PE spectroscopy allow us to calculate the so called skin depth δ[16] and estimate how deep the EM waves penetrate the surface of the metal. For optical wavelengths between 200 and 800 nm and assuming a typical mean free time of $2x10^{-14}$ s between conduction band electron collisions, we find that δ_{MW} for the metallic water solution ranges from 3.7 – 7.4 nm and δ_{NaK} for NaK ranges from 2.0 – 4.1 nm. EM radiation is thus effectively reflected within the first 15 – 25 or 10 – 15 monolayers of the metallic water solution or NaK, respectively. These differences also indicate that when probing the light–matter interaction of the metallic water layer on the NaK surface, three spectral intervals need to be distinguished (see scheme in Figure S13b):

Exposing NaK drops to water vapour induces a colour change (from silver to yellow with a golden metallic sheen) that we can probe using optical spectroscopy. The colour of metals interacting with electromagnetic (EM) radiation is determined[15] by their plasmon resonance frequency (ω_P), as smooth metal surfaces will reflect EM radiation with frequencies ω up to the plasmon resonance frequency ($\omega \leq \omega_P$) and become transparent

beyond this (i.e., $\omega > \omega_P$; see scheme in Figure S13a). Pure NaK, consisting of two simple metals, has no optical inter-band transitions and thus no visible light absorption[12].

Upon exposure to water, a layer of a metallic solution forms on the NaK drop and grows in thickness at a rate of ~24 nm/s (see main text). Within the first ~5 seconds during which the drop is gold-coloured, the metallic solution thus reaches a thickness of ~120 nm that is below the 200-800 nm wavelength range used in our optical investigations. The free electron densities determined by PE spectroscopy allow us to calculate the so called skin depth δ[16] and estimate how deep the EM waves penetrate the surface of the metal. For optical wavelengths between 200 and 800 nm and assuming a typical mean free time of 2×10^{-14} s between conduction band electron collisions, we find that δ_{MW} for the metallic water solution ranges from 3.7 – 7.4 nm and δ_{NaK} for NaK ranges from 2.0 – 4.1 nm. EM radiation is thus effectively reflected within the first 15 – 25 or 10 – 15 monolayers of the metallic water solution or NaK, respectively. These differences also indicate that when probing the light–matter interaction of the metallic water layer on the NaK surface, three spectral intervals need to be distinguished (see scheme in Figure S13b):

1. $\omega < \omega_{MW}$: light with photon energies smaller than 2.7 eV (λ_{MW} = 460 nm) is reflected directly from the surface of the metallic water solution.

2) $\omega \approx \omega_{MW}$: one would expect the metallic water layer to become transparent for light with frequencies around and above ω_{MW} due to the plasmon cutoff in reflectivity. The transmitted light would however be reflected from the underlying NaK surface since the plasmon frequency of NaK is at a higher photon energy of ~4.5 eV (~260 nm). One would not expect any light absorption as bulk plasmons do not not generally interact with incident light[15]. Namely, plasmons as longitudinal waves do not couple to transverse EM waves. Instead, plasmons are typically excited by particle impact, e.g., in electron scattering processes pertinent to the above PE spectroscopy.

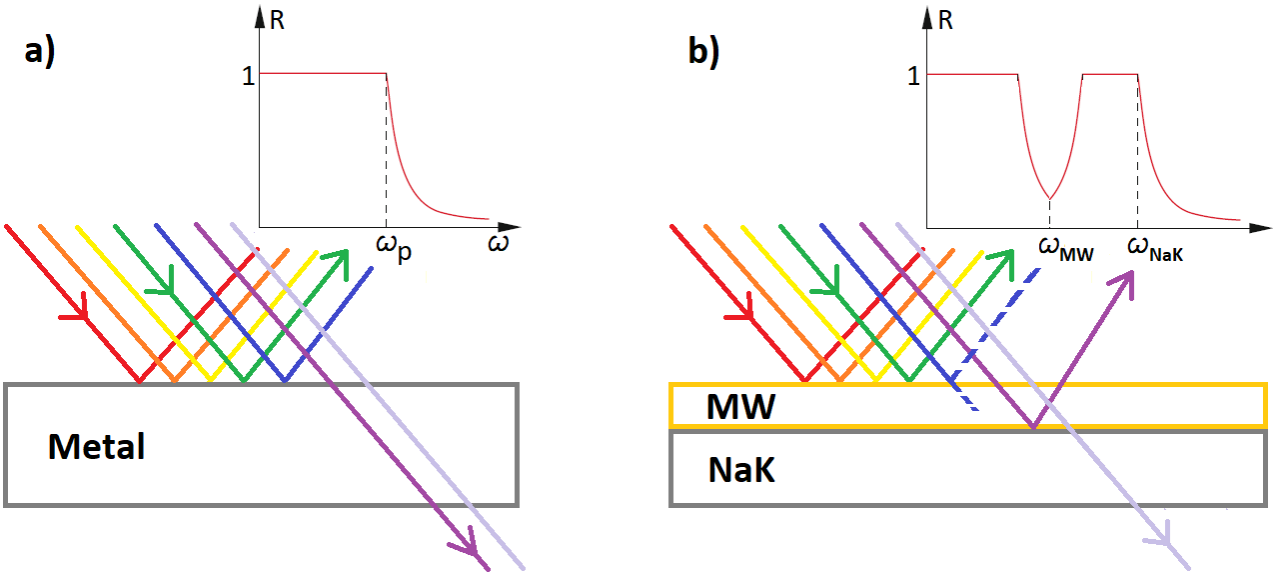

Figure S13: Schematic picture of the characteristics of light interacting with a smooth metal surface. It shows how visible and UV light is reflected and transmitted from a) surface of a bulk metal and b) metallic water solution on top of NaK, if the frequency (ω) of of the EM radiation is smaller or larger than the plasmon resonance frequency (ω_P).

In very thin metallic layers, however, optical excitation of a plasmon becomes possible[17-19]. Namely, if EM radiation is incident upon a very thin metal slab with an electric field component normal to the metal surface, then there can be a coupling between the free electron plasma and the EM wave, which is most pronounced if the metal film has a thickness around a half of the wavelength corresponding to the plasmon energy[20]. In the present case, the metallic water solution thus should not be thicker than $\lambda_{MW}/2 \leq 230$ nm, which is definitely the case within the ~5 seconds of existence of the gold-coloured layer.

The interaction can be rationalized as follows[21]: The electric field component normal to the surface of the metallic water layer causes a collective displacement of the electrons along the surface normal following the oscillation of the EM radiation, which causes surface charging on the sides of the metal layer. The interaction between the

oscillating frequency of the EM wave and the excitation of the electron plasma can be described using the model of an externally driven harmonic oscillator model[18], where the strongest coupling occurs under a resonance condition ($\omega \approx \omega_P$). Electron-electron collisions and Landau damping[15] effectively lead to absorption of photons which is measured here as a dip around the plasmon frequency ω_P. Also, for the thin metallic water layer on the NaK surface we do not expect significant interaction between the two free electron gases of the two metals since their plasmon frequencies are very different and are not multiples of each other[19].

3. $\omega_{NaK} > \omega > \omega_{MW}$: the incoming light is transmitted through the metallic water layer and reflected from the underlying NaK surface. Hence, the reflected intensity increases up to almost unity for light with frequencies larger than $\omega_{MW,}$ up to the NaK plasmon energy of ~4.5 eV (beyond which the reflection probability would decrease as both metals become transparent).

The setup of a metallic water layer on a NaK surface allows us to measure the absorption band of its plasmon directly since we are measuring the reflection and the transmission spectrum of the metallic water layer simultaneously, with the advantage of the absorption being enhanced as light with frequencies ~ω_{MW} is passing through the metallic water layer twice (see Figure S13b). These considerations allow us to assign the minimum of the absorption band directly to the plasmon frequency of the metallic water solution and to fit the absorption band by a Lorentzian function which models optical damping due to the coupling to the plasmon[18].

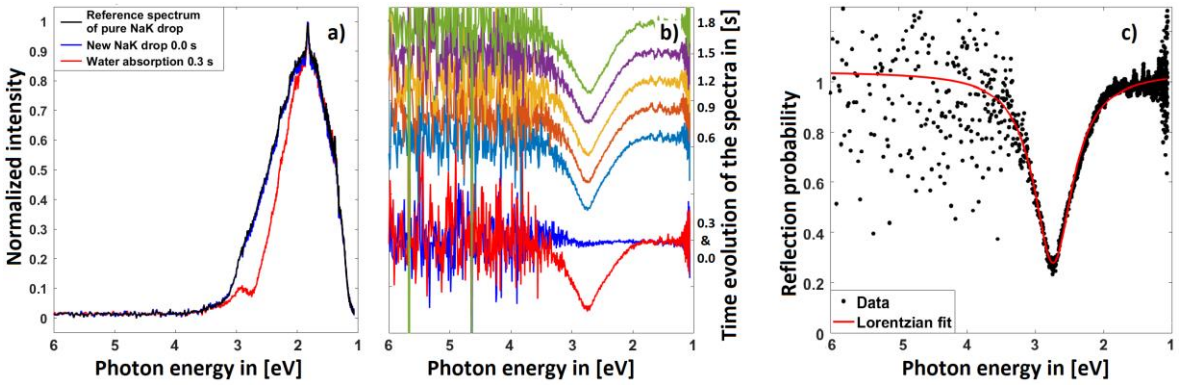

Figure S14: a) Normalized spectral intensity distribution as a function of the photon energy – the reference spectrum plotted in black depicts the reflection of the broadband white light source from the pure NaK drop. The blue line shows the reflected spectral intensity distribution of a newly emerging NaK drop defining 0.0 s, while the red line depicts the spectrum of the drop after being exposed to water vapour for 0.3 s – the spectral absorption dip around 2.7 eV is already very prominent. b) Time evolution of the difference spectra sampled as the drop is exposed to water vapour with a time interval of 0.3 s - the plasmon absorption around 2.7 eV remains roughly constant for the first two seconds. c) Example of fitting of a Lorentzian function to the data.

Figure S1b shows schematically how the optical reflection measurements were conducted. A glass apparatus was evacuated to 10^{-5} mbar. A boro-silicate flask was mounted as the NaK container from the top, while the main optical access was given via a CaF_2 window from the side. This allowed investigation of the NaK drop hanging at the quartz capillary within a large solid angle of ~40°. We illuminated the drop with a 100-watt tungsten incandescent light bulb. The reflected light from the NaK drop was collected and imaged into an optical fiber using two lenses. To ensure that we collect reflected light from a spot smaller than ~1 mm^2 on the NaK drop, we shone a laser pointer through the optical fiber and the lens system onto the drop, where the light was reflected from the NaK drop towards the light bulb. Once the optics were correctly aligned, the

optical fiber was screwed into a spectrometer (AvaSpecULS 2048) – this spectrometer allows the simultaneous acquisition of the spectral range of 200 – 1100 nm. The experimental setup and a typical measurement is further described in detail in a Supplementary Video[22].

We synchronized the data acquisition using Open Broadcaster Software (OBS studio 25) where we framed the graphical user interfaces of the spectrometer software, the CCD camera and the current time stamp of the computer at a rate of 0.1 frames per second. Meanwhile, the individual software components were recording, e.g., the spectrometer software acquired spectra at a rate of one spectrum every 0.3 s. These data were directly saved in a file together with the corresponding time stamp. In each experimental run, we first took spectra of pure NaK drops without any water vapour present. These spectra were first averaged and then normalized in order to determine a reference spectrum of the white light source reflected from the surface of a pure NaK drop. Its spectral intensity distribution is plotted as a function of the photon energy as solid black line in Figure S14a.

In order to reconstruct the time evolution of the spectrum and hence the progression of the colour change of the drop we correlated the visual evidence from the CCD camera with the saved spectral data sets using the common time stamp. In this way, we can also determine the moment where an old drop has just fallen off and a new drop starts emerging. The blue line in Figure S14a shows the normalized reflected spectral intensity distribution of a newly emerging NaK drop defining t = 0.0 s, while the red line depicts the spectrum recorded after the drop was exposed to water vapour for 0.3 s. Here, the spectral absorption band around 2.7 eV is already very prominent.

Figure S14b illustrates how we evaluated the reflection probability as a function of the photon energy. The individual normalized spectra taken at 0.0 s and 0.3 s (blue and red lines in Figure S14a) were divided by the reference spectrum (black line in Figure

S14a). The blue and red lines in Figure S14b show the normalized reflection probability for the spectra in Figure S14a. The blue spectrum of the newly emerging NaK drop shows no absorption feature, hence the timing of 0.0 s is absolutely justified. The red spectrum recorded 0.3 s later already shows a symmetric absorption feature around 2.7 eV. The upper part of Figure S14b shows the spectra recorded at later times sampled every 0.3 s. The temporal evolution of the spectra illustrates that the symmetric absorption feature around 2.7 eV is not shifting as long as the colour of the drop remains golden.

In order to determine the minimum and the width of the plasmon absorption band, we fit a Lorentzian function[18,21] to the individual spectra:

$$\mathrm{Lor}(E_{\mathrm{ph}}) = \mathrm{A}_A \left(\frac{\Gamma}{(E_{\mathrm{ph}} - E_A)^2 + \Gamma^2} \right),$$

where A_A, Γ, and E_A are fitting parameters accounting for the amplitude, width, and position of the centre of the distribution, respectively. Figure S14c shows an example of the fitting of a Lorentzian function to the data recorded at 0.3 s corresponding to the red line data set in Figure S14b. The Lorentzian function fits the data very well revealing a minimum and a width of the absorption feature to be 2.74 and 0.59 eV, respectively. The fitted results compare quantitatively to the analogous fits to PE spectra, see Table S1.

8. References

1 Mason, P. E., Uhlig, F., Vanek, V., Buttersack, T., Bauerecker, S. & Jungwirth, P. Coulomb explosion during the early stages of the reaction of alkali metals with water. *Nature Chemistry* **7**, 250-254, doi:10.1038/nchem.2161 (2015).

2 Buttersack, T., Mason, P. E., McMullen, R., Schewe, H. C., Martinek, T., Brezina, K., Crhan, M., Gomez, A., Hein, D., Wartner, G., Seidel, R., Ali, H., Thurmer, S., Marsalek, O., Winter, B., Bradforth, S. E. & Jungwirth, P. Photoelectron spectra of alkali metal-ammonia microjets: From blue electrolyte to bronze metal. *Science* **368**, 1086-1091, doi:10.1126/science.aaz7607 (2020).

3 Waseda, Y., Jacob, K. T., Tsuchiya, Y. & Tamaki, S. Vapor-Pressure of Liquid-Metals and Alloys. *Zeitschrift Fur Naturforschung Section a-a Journal of Physical Sciences* **33**, 940-945 (1978).

4 Sawhney, K. J. S., Senf, F. & Gudat, W. PGM beamline with constant energy resolution mode for U49-2 undulator at BESSY-II. *Nuclear Instruments &*

Methods in Physics Research Section a-Accelerators Spectrometers Detectors and Associated Equipment **467**, 466-469, doi:10.1016/s0168-9002(01)00360-6 (2001).
5 Seidel, R., Pohl, M. N., Ali, H., Winter, B. & Aziz, E. F. Advances in liquid phase soft-x-ray photoemission spectroscopy: A new experimental setup at BESSY II. *Review of Scientific Instruments* **88**, doi:10.1063/1.4990797 (2017).
6 Buttersack, T., Mason, P. E., Jungwirth, P., Schewe, C., Winter, B., Seidel, R., McMullen, R. & Bradforth, S. E. Deeply Cooled and Temperature Controlled Microjets: Liquid Ammonia Solutions Released into Vacuum for Analysis by Photoelectron Spectroscopy. *Review of Scientific Instruments* **91**, 043101, doi:DOI: 10.1063/1.5141359 (2020).
7 Bonzel, H. P., Pirug, G. & Winkler, A. Adsorption of H2O on Potassium Films. *Surface Science* **175**, 287-312, doi:10.1016/0039-6028(86)90237-2 (1986).
8 Citrin, P. H. High-Resolution X-Ray Photoemission from Sodium Metal and its Hydroxide *Physical Review B* **8**, 5545-5556, doi:10.1103/PhysRevB.8.5545 (1973).
9 Petersson, L.-G. & Karlsson, S.-E. Clean and Oxygen Exposed Potassium Studied by Photoelectron Spectroscopy. *Physica Scripta* **16**, 425 (1977).
10 Winter, B., Faubel, M., Vacha, R. & Jungwirth, P. Behavior of hydroxide at the water/vapor interface. *Chemical Physics Letters* **474**, 241-247 (2009).
11 Winter, B., Weber, R., Widdra, W., Dittmar, M., Faubel, M. & Hertel, I. V. Full valence band photoemission from liquid water using EUV synchrotron radiation. *Journal of Physical Chemistry A* **108**, 2625-2632 (2004).
12 Kittel, C. *Introduction to Solid State Physics*. (John Wiley & Sons, Inc., 2005).
13 Thompson, J. C. *Electrons in Liquid Ammonia*. (Clarendon Press, 1976).
14 Hufner, S. *Photoelectron Spectroscopy, Principles and Application*. (Springer, 2003).
15 Maier, S. *Plasmonics – Fundamentals and Applications*. (Springer, 2007).
16 Demtroeder, W. *Experimental Physics 2, vol. 7*. (Springer, 2017).
17 Raether, H. *Springer Tracts in Modern Physics, vol. 38*. (Springer, 1965).
18 Nilson, P. O., Lindau, I. & Hagstrom, S. B. Optical Plasma-Resonance Absorption in Thin Films of Silver and Some Silver Alloys. *Physical Review B* **1**, 498 (1970).
19 Steinmann, W. Optical Plasma Resonances in Solids. *Physica Status Solidi* **28**, 437 (1968).
20 Ferrell, R. A. Predicted Radiation of Plasma Oscillations in Metal Films. *Physical Review* **111**, 1214 (1958).
21 McAlister, A. J. & Stern, E. A. Plasma Resonance Absorption in Thin Metal Films. **132**, 1599 (1963).
22 Mason, P. E. *Supplementary Video: Optical Spectroscopy Setup*, <https://www.dropbox.com/s/bhewrq6jrafe79h/running%20the%20nak%20kit%20v3%20720.mp4?dl=0> (2020).